Precisely Engineered Interactions between Light and Ultracold Matter

M. M. Boyd, A. D. Ludlow, S. Blatt, G. K. Campbell, T. Zelevinsky, S. M. Foreman, and J. Ye

JILA, National Institute of Standards and Technology and University of Colorado
Department of Physics, University of Colorado, Boulder, CO 80309-0440, USA
Web http://jilawww.colorado.edu/YeLabs/; Email Ye@jila.colorado.edu

Summary. — Modern capabilities in quantum state engineering of ultracold matter and precise control of light fields now permit accurate control of interactions between matter and field to suit applications for precision tests of fundamental physics. We report on our recent development of a highly stable and accurate optical atomic clock based on ultracold neutral Sr atoms confined in an optical lattice. We discuss precision tools for the lattice clock, including stabilized lasers with sub-Hz linewidth, femtosecond-comb based technology allowing accurate clock comparison in both microwave and optical domains, and clock transfer over optical fibers. With microkelvin Sr atoms confined in an optical lattice that provide a zero differential a.c. Stark shift between two clock states, we achieve a resonance quality factor $>2\times10^{14}$ on the $^1S_0 - ^3P_0$ doubly forbidden ^{87}Sr clock transition at 698 nm. High resolution spectroscopy of spin-polarized atoms is used for both high-performance clock operations and accurate atomic structure measurement. The overall systematic uncertainty of the clock has been evaluated at the 10^{-16} level, while the stability approaches low 10^{-15} at 1 s. These developments in precise engineering of light-atom interactions can be extended to the field of ultracold molecules, bringing new prospects for precision measurements, quantum control, and determinations of the constancy of the fundamental constants.

1. – Introduction - the Quest for Coherence of Light-Matter Interactions

The quest for spectroscopic resolution has stimulated many scientific and technological breakthroughs, including the invention of the laser and the realization of ultracold atoms. Lasers with state-of-the-art frequency control now maintain optical phase coherence over 1 s [1, 2]. The recent development of optical frequency combs [3, 4] has allowed this optical phase coherence to be precisely transferred to other optical or microwave spectral domains [5, 6]. To preserve the longest possible coherence times between atomic states and an optical field, the atomic center-of-mass motion needs to be understood and controlled at the scale of an optical wavelength. Furthermore, optical probing of internal atomic

states creates an inevitable back-action on the atomic center-of-mass motion due to non-negligible photon recoil momentum, further limiting measurement precision and control.

Atomic localization within a fraction of an optical wavelength in a deeply bound trap is thus desirable for the removal of atomic motional effects from optical spectroscopy and state control. In this Lamb-Dicke regime [7], the Doppler effect is greatly reduced and photon recoils are removed as the trap frequency exceeds the recoil. The quantized atomic motion and long interrogation times in the trap permit high-resolution and precise investigations. These capabilities have long been utilized in trapped ion systems where charged ions are deeply bound with minimal perturbations to their electronic states [8]. The separation of internal and external dynamics is critical for precision measurement, frequency metrology, coherent manipulations of quantum systems, and the broad scope of quantum information science.

Many protocols for precision measurement and quantum information science call for a large ensemble of neutral atoms to either boost the measurement signal-to-noise ratio (S/N), explore the atomic collective effects, or to create a massively entangled system. For neutral atoms, external trapping potentials are created from spatially inhomogeneous energy shifts of the electronic states produced by an applied magnetic, electric, or optical field. In general, such energy shifts are electronic-state dependent, and hence atomic motion results in dephasing of the two states.

Optical traps [9, 10] employ a.c. Stark shifts $U_T = -\frac{1}{2}\alpha(\lambda,\varepsilon)|\vec{E}(\vec{r},\lambda,\varepsilon)|^2$ introduced by a spatially inhomogeneous light field of $\vec{E}(\vec{r},\lambda,\varepsilon)$, with $\alpha(\lambda,\varepsilon)$ the polarizability, λ the wavelength, and ε the light polarization. Two atomic states of interest generally have different α_i (i = 1, 2), resulting in correspondingly different external potentials U_{Ti}. To preserve the atomic coherence between these two states despite atomic motion, a state-insensitive optical trap can be designed where under a specific (termed "magic") wavelength and polarization state, $\alpha_1(\lambda_M,\varepsilon_M) = \alpha_2(\lambda_M,\varepsilon_M)$, and thus $U_{T1}(\vec{r}) = U_{T2}(\vec{r})$ [11, 12, 13]. Consequently, the transition frequency between the two electronic states becomes nearly decoupled from the position-dependent field $\vec{E}(\vec{r},\lambda,\varepsilon)$, so long as higher order contributions ($|\vec{E}|^4$ and higher) are negligible. This scenario is possible since the wavelength and polarization dependence of the polarizability are influenced by multiple off-resonant transitions present in a multilevel atomic system.

The state-insensitive optical trap permits independent measurement of atomic transition and atomic center-of-mass motion [13]. Combined with the condition that atoms are trapped in the Lamb-Dicke regime, an ensemble of these neutral atoms emulates multiple parallel traps of single ions, creating enhanced capabilities for measurement and control. This scenario is obviously attractive for an array of experiments for quantum information science [14] and precision frequency metrology [15], both demanding that coherence times for matter-field interactions far exceed the decoherence time and that external trapping potentials not compromise the probe of the intrinsic system eigenlevel structure.

2. – Optical Frequency Standard with Trapped Atoms

Enabled by a clean separation between the internal and external degrees of freedom for trapped atoms, a new generation of atomic clocks based on optical transitions that have surpassed the primary Cs standard has been developed [16, 17]. A premier example is optical frequency standards based on single-trapped ions. In particular, the overall systematic uncertainty of the Hg^+ [16] standard of the National Institute of Standards

and Technology (NIST) has been evaluated below 10^{-16}, surpassing the present performance of primary Cs fountains. A key feature of the trapped-ion-based clocks is the Lamb-Dicke [7] confinement provided by the trap. The quantized motion provides an absorption spectrum in which the atomic resonance is neither broadened nor shifted, but instead modulated by motional sidebands. The resulting spectrum is a strong central carrier at the natural transition frequency with small sidebands located at integer multiples of the trap frequency [18, 19]. The problem of atomic motion is then transformed to one of line pulling from the motional sidebands that in most systems are negligible at the relevant level of accuracy.

The performance of a frequency standard is usually characterized by its accuracy, reproducibility, and stability. Accuracy is associated with the overall systematic uncertainty and it refers to the intrinsic property of a standard to maintain the value of an atomic transition frequency when the atoms are free of any perturbation. Similar to trapped ion standards, the magic-wavelength optical trap for neutral atoms provides the capability to decouple the external (motional) and internal (atomic state) degrees of freedom. The differential frequency shifts between two clock states are eliminated, resulting in systematic uncertainties currently evaluated at $\sim 10^{-16}$ [17]. Reproducibility is a measure of the degree to which a frequency standard repeats itself from unit to unit and upon different realizations. Again, the magic-wavelength optical trap provides a strong safeguard for independence from details of experimental operations. Finally, stability represents the repeatability of the measured clock frequency over a given averaging time τ. It is also referred to as the level of precision for an atomic clock. The stability is typically expressed as the Allan deviation, in fractional frequency units, given as [20]

$$\sigma_y(\tau) = \frac{\delta\nu(\tau)_{rms}}{\nu} = \frac{\chi}{2\pi Q\, S/N}\sqrt{\frac{t_c}{\tau}}. \tag{1}$$

Here, $Q\,(=\nu/\Delta\nu)$ is the line quality factor of the clock transition for a linewidth $\Delta\nu$, S/N is the signal-to noise-ratio achieved in the measurement cycle time t_c, and χ is a constant of order unity that depends on the transition lineshape used for measurements. For quantum projection noise limited measurements, the S/N is determined by the number of atoms (N_a) used in each measurement, as $\sqrt{N_a}$. Clearly, the combined product of line Q and S/N is the major deciding factor for clock performance, as it controls the time scale within which a certain measurement precision can be obtained. The high line Q's offered by state of the art optical clocks [21, 22] should allow dramatic improvement in precision. The use of a large ensemble of neutral atoms confined in a magic wavelength optical lattice offers the other important improvement factor, i.e., S/N. A more precise clock is attractive for the characterization of its overall accuracy since its systematic uncertainties can be evaluated more quickly.

3. – Confined Neutral Atoms and the Stark Cancelation Technique

Optical clocks based on neutral atoms tightly confined in optical lattices have recently begun to show bright prospects as future time/frequency standards [23, 24, 25, 26, 21, 27, 28, 29, 30, 17]. These optical lattice clocks enjoy a relatively high S/N via the use of large numbers of atoms, while at the same time allowing Doppler- and recoil-free interrogations of the clock transition for long probing times [21], a feature typically associated with single trapped ions.

Alkaline earth(-like) species offer the most attractive choice for neutral-atom-based clocks. The double valence electrons give rise to two distinct series of singlet and triplet states, resulting in long-lived metastable states that are suitable for precision spectroscopy and metrology [31]. In the case of Sr, intercombination optical transitions from the ground state $5s^2\ {}^1S_0$ to the lowest ${}^3P_{0,1,2}$ metastable states have narrow linewidths that are suitable for clock transitions [32, 15]. As transitions between pure scalar states are strictly forbidden, the existence of a nuclear spin is necessary to introduce hyperfine interaction-mediated states, such as ${}^3P_0(F = I)$, with F the total angular momentum and I the nuclear spin. In ^{87}Sr, $I = 9/2$ very weakly permits the spin- and dipole-forbidden ${}^1S_0(F = I) - {}^3P_0(F = I)$ transition with a natural linewidth of 1 mHz [33, 34, 29], corresponding to an exceedingly high Q for the optical resonance.

To take full advantage of Eq. 1, long coherence times should be established for the interaction between many atoms and the probe light field. Laser cooled atoms confined in an optical lattice can realize the condition of Lamb-Dicke confinement. The presence of a strong spin-singlet ${}^1S_0 - {}^1P_1$ transition and a weak spin-forbidden ${}^1S_0 - {}^3P_1$ transition in Sr allows efficient laser cooling in two consecutive stages [35], reaching high atomic densities and low temperatures limited by photon recoils ($<1\ \mu$K) [36]. All of the relevant light sources required for cooling and trapping, repumping, and spectroscopy can be generated from inexpensive diode laser sources [37].

Typically, however, the polarizabilities of the two clock states are different such that their differential a.c. Stark shifts inside the optical trap causes the clock transition to deviate from its nominal frequency value. Furthermore, as the trap intensity is inhomogeneous, atomic motions within the trap couple the external and internal degrees of freedom, degrading the coherence in spectroscopic measurement. This problem is particularly pressing with the intercombination transitions in alkaline earth atoms as the resonance linewidths are significantly narrower than typical a.c. Stark shifts.

It is thus critical to find an optical trapping wavelength where the polarizabilities of the two clock states are matched. Besides offering an ultra narrow linewidth, the ${}^1S_0 - {}^3P_0$ transition in ^{87}Sr is well suited for such a scheme as the nearly independent series of singlet and triplet states permit the Stark shift of ${}^1S_0$ and ${}^3P_0$ to be tuned semi-independently. The use of electronic scalar states ($J = 0$) allows precise characterization of Stark effects primarily by the light wavelength, with a drastic reduction of the light polarization dependence and many other systematic effects [15]. Using optically cooled ^{87}Sr atoms in a zero-differential-Stark-shift, one dimensional (1D) optical lattice and an ultrastable probe laser with a sub-Hz line width, we have experimentally obtained transition linewidths below 2 Hz [21]. This represents a fractional resolution of $\sim 4 \times 10^{-15}$. Consequently, the systematic uncertainty of the clock is currently evaluated at $\sim 1 \times 10^{-16}$ [17].

3˙1. *Magic Wavelength Optical Lattice.* – To find an optical trapping wavelength that provides equal a.c. Stark shifts for ${}^1S_0$ and ${}^3P_0$, along with negligible scattering losses, we need to carefully examine the wavelength and polarization dependence of the dynamic polarizabilities of the two clock states, which are influenced by multiple off-resonant transitions. In Sr, for optical wavelengths longer than 461 nm, the polarizability of ${}^1S_0$ is always positive and hence a trapping potential is formed at the intensity maximum. For ${}^3P_0$, however, the resonances at 2.7 μm and 0.68 μm dictate that its polarizability varies from largely negative to largely positive values as the wavelength decreases. This guarantees a crossing of the ${}^1S_0$ and ${}^3P_0$ polarizabilities at a magic wavelength value, as shown in Fig. 1.

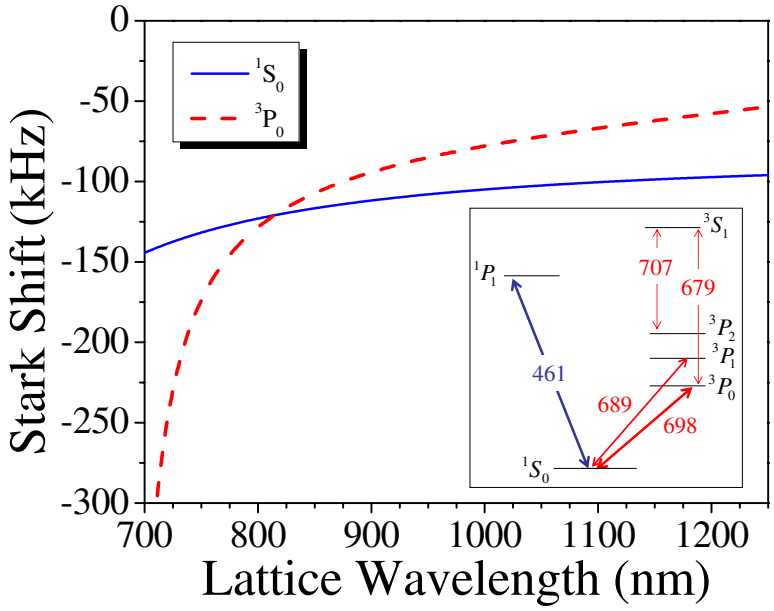

Fig. 1. – Calculated wavelength dependent a.c. Stark shifts of the $^3P_0$ (dashed line) and $^1S_0$ (solid line) Sr clock states for a laser intensity of 2.2 kW/cm^2. The inset shows the relevant Sr energy level diagram and optical transitions for this work. The $^1S_0$–$^1P_1$ and $^1S_0$–$^3P_1$ transitions are used for laser cooling to μK temperatures while the $^3S_1$ state is used for optical pumping inside the blue magneto-optical trap (MOT) and later for spectroscopy normalization. Transition wavelengths are given in nanometers.

The Stark-cancelation wavelength, or magic wavelength, for the optical lattice occurs at a very convenient wavelength which has been measured to be 813.428 nm [23, 24, 38]. Figure 1 shows calculations of the wavelength-dependent light shifts of the two clock states [39]. The level shifts are identical at a wavelength of 815 nm, close to the experimental value. To predict the magic wavelength, we sum contributions from electronic states that have dominant dipole couplings to $^1S_0$ and $^3P_0$, respectively, with details provided in Ref. [39]. When electronic states with nonvanishing electronic angular momentum ($J \neq 0$), for example, $^3P_1$ is used as an upper clock state, then the vector nature of the state makes the a.c. Stark shift dependence on the light polarization much more complex.

Confined within a magic-wavelength optical lattice of a sufficient depth, atomic transitions are measured without Stark shifts or Doppler and recoil effects, leading to a clean separation of the atomic motion from the internal degrees of freedom. This scenario is similar to a trapped ion system, but with many more atoms available for spectroscopy.

3˙2. *Considerations for the Optical Lattice.* – While the magic-wavelength lattice provides an equal a.c. Stark shift for $^1S_0$ and $^3P_0$, the $^3P_1$ state experiences a different shift. However, the two shifts are of the same sign and their difference is well within the frequency tuning range for efficient laser cooling via $^1S_0$–$^3P_1$. Thus, the lattice can coexist with the red MOT and laser-cooled and trapped atoms are continually loaded into the lattice.

The 1D optical lattice is formed by an optical standing wave with its axis oriented in the vertical direction. The resulting potential difference between neighboring lattice sites, i.e., $m_{Sr}\ g\ \lambda_M/2$, removes the degeneracy of the otherwise translation-symmetric lattice sites. Here, g is the Earths gravity induced acceleration. The formation of localized Wannier-Stark states strongly inhibit tunneling between lattice sites, eliminating a potential problem of accuracy for the optical lattice clock [40]. Due to the existence of nuclear spin, the two clock states $^1S_0$ and $^3P_0$ are not purely scalar. The Stark shifts cannot be completely compensated for all of the magnetic sublevels simultaneously. Or equivalently, the magic wavelength will be slightly different depending on the sublevel used [27, 29]. The magnitude of this effect is rather small for $^1S_0$ and $^3P_0$ states and can be effectively controlled. Typically, for the 1D lattice, the laser polarization is linear and coincides with a transverse magnetic field (if it is used to lift the spin degeneracy) to jointly define the quantization axis.

The typical lattice trap depth is 30-50 photon recoil energy, sufficient to confine atoms in the Lamb-Dicke regime, as the axial trap frequency (tens of kHz) far exceeds the photon recoil (5 kHz), resulting in recoil-free atomic absorptions. The probe is aligned precisely parallel to the lattice axis to avoid transverse excitations and the probe polarization is parallel to that of the lattice laser. The Doppler effect is quantized due to the periodic atomic motion and is removed completely via resolved-sideband spectroscopy where the trap frequency is much greater than the narrow linewidth of the clock transition probed by a highly coherent laser. The use of the magic wavelength allows atoms confined in the perturbation-free lattice to preserve the coherence of the $^1S_0$ and $^3P_0$ superposition for 1 s [21].

4. – Optical Clockwork

4˙1. *Stable Optical Local Oscillator.* – For the purpose of operating an optical clock with the best possible stability, it is necessary for the probe laser to have an exceedingly long phase-coherence time. Development of such an oscillator to probe the Sr clock transition at 698 nm has therefore been one of the central focuses of our work. The stabilization scheme for our laser is discussed in detail elsewhere [2]. Briefly, a grating-stabilized diode laser is locked to a high-finesse ultra-low-expansion (ULE) cavity mounted in a vertical orientation to reduce fluctuations of the cavity length due to vibrations [41]. The cavity is under vacuum and mounted on a compact, passive vibration-isolation table.

The clock laser performance has been characterized in a number of ways, including direct comparison of two similar systems at 698 nm, comparison to highly stabilized lasers at other colors using the fs-comb, and by precision atomic spectroscopy. Direct comparison between the two 698 nm systems via heterodyne beat reveals narrow linewidths often below 300 mHz for integration times of a few seconds (see the inset of Fig. 2). For integration times on the scale of minutes the beat linewidth typically broadens to a few Hz. The drift of the ULE cavity is typically on the order of 300 mHz/s. The Allan deviation shown in Fig. 2 reveals that the fractional frequency noise of the beat is $\sim 1 \times 10^{-15}$ at 0.1 - 100 s, consistent with the expected limit set by thermal-mechanical noise in the cavity mirrors and mirror coatings [42, 43].

4˙2. *Optical Frequency Comb Clockwork and Precision Fiber Transfer.* – The femtosecond optical comb plays an essential role for clock development. It provides a coherent link between high accuracy clocks operating in either the optical or microwave domains. For absolute frequency measurements, a direct-octave-spanning, self-referenced frequency

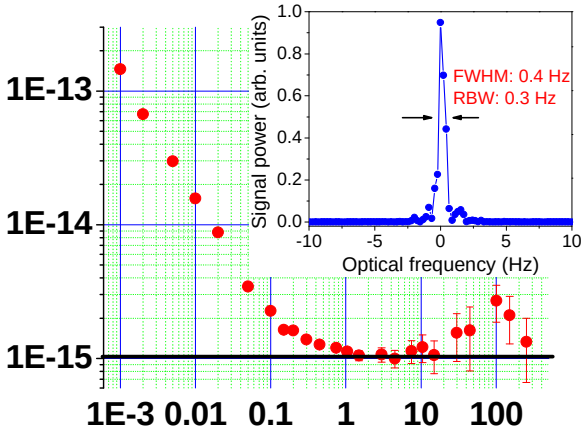

Fig. 2. – Allan deviation (with a linear drift removed) for a heterodyne beat between two independent clock lasers at 698 nm. The $\sim 1 \times 10^{-15}$ stability at 0.1 - 1000 s is consistent with the estimated thermal noise limit. The inset shows a beat signal between the two lasers below 1 Hz linewidth for an integration time of a few seconds.

comb is stabilized by the clock laser at 698 nm [6]. The comb provides a measurement of the laser frequency relative to a microwave signal derived from a hydrogen maser calibrated to the NIST primary Cs fountain clock [44]. To enable the microwave comparison, a diode laser operating near 1320 nm is amplitude-modulated and transmitted over a 3.5-km fiber optic link from NIST to JILA [45]. The instability of the frequency-counting signal is $\sim 2.5 \times 10^{-13}$ for a 1-s integration time [46]. The periodic stretching and compressing of the fiber, associated with daily temperature cycles, has been found to cause frequency offsets as large as 10^{-14}. Stabilization of the fiber link is thus implemented for high accuracy clock comparisons.

The comb and fiber link also support transmission of stable optical frequencies between JILA and NIST [6]. First, the comb is used to distribute the Sr clock stability across the optical spectrum, allowing use of a transfer laser at 1064 nm. We have examined the precision of the distribution across the comb spectrum by comparing our 698 nm clock laser with a similar independent system operating at 1064 nm. The resulting beat between the stabilized comb and the 1064 nm laser has a linewidth below 0.5 Hz, verifying the ability of the comb to fully preserve the optical phase coherence across the visible spectrum. For transfer of the clock signal, a 1064 nm laser is phase-locked to the comb and sent through the fiber to the NIST laboratory where it is measured relative to a number of high accuracy optical clocks using a second fs-comb [47]. To eliminate noise induced by the transfer, the 1064 nm light is partially reflected back to the JILA laboratory allowing interferometric stabilization of the link. Figure 3(a) shows a beat between the transfer laser and a NIST fs-comb that is stabilized to a local oscillator used for the Hg^+ clock [1]. The beat has a resolution-bandwidth-limited linewidth of 1 Hz, demonstrating that the phase coherence of the two clock lasers is not degraded by the two fs-combs and the fiber transfer process. In addition, Fig. 3(b) summarizes results of passive and phase-stabilized optical transfer for 7 km (the round trip length of our fiber link) and 32 km fiber lengths. The transfer noise of the stabilized fiber links is $\sim 1 \times 10^{-17}$ at 1 s.

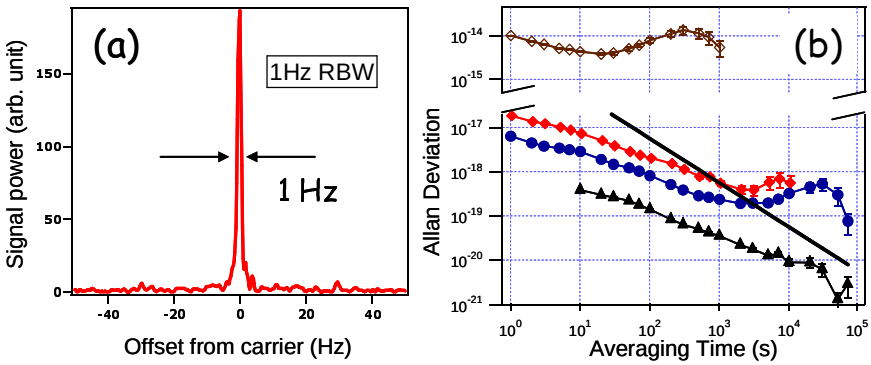

Fig. 3. – (a) Optical beat between the fiber-transferred laser and the NIST comb at 1064 nm. The fs-comb in JILA is stabilized to the 698 nm clock laser, distributing the stability across the optical spectrum. A JILA 1064 nm Nd:YAG laser is stabilized to the comb and used as a transfer laser to NIST over a 3.5 km fiber which is optical-phase stabilized. At NIST, a second fs-comb stabilized to the 1123 nm Hg^+ clock laser is used to compare the two stable oscillators. The beat linewidth between the NIST comb and the transfer laser is 1 Hz. (b) Instability of the transfer systems. Open diamonds are typical passive instabilities of the 7- and 32-km fiber links. Closed diamonds (circles) are for the 32-km (7-km) fiber transfer system. Triangles represent in-loop performance. The solid line represents 1 radian of accumulated phase noise during the averaging time.

5. – High Resolution Spectroscopy of Confined Atoms

Precision spectroscopy of confined atoms inside a magic-wavelength trap provides a unique spectrum of information. When the transition is strongly saturated, spectra such as that in Fig. 4 are observed. When the probe laser frequency is scanned, a carrier transition appears without change of the motional state. Blue and red-detuned motional sidebands appear on either side of the carrier, resulting from corresponding changes of the motional states by ± 1. The sideband spectrum is useful for direct measurement of the thermal-mechanical properties of the trapped atoms, including temperatures and trap oscillation frequencies. The relative height of the red and blue detuned sidebands gives information about the atomic temperature along the lattice axis. In the trace shown in Fig. 4, the red sideband is strongly suppressed since most of the atoms are already in the ground motional state. The asymmetrical lineshape of the sidebands arises from the radial motion in the trap that allows the atoms to sample different intensity regions of the transverse gaussian profile [24, 39], as well as the anharmonicity of the trapping potential that results in an n-dependant trap frequency.

The narrow central feature is of most interest for an atomic reference as it is the absorption feature which does not include any motional or Stark broadening when the magic wavelength condition is achieved. To test the spectroscopic limits of the lattice clock, high-resolution spectroscopy is performed on time scales approaching 1 s. To ensure the narrowest atomic signal is observed, the degeneracy of the clock states is lifted by applying a magnetic field, so that the spin-resolved transitions can be explored free of broadening from state-dependent Zeeman and Stark shifts. Examples of transition spectra are shown in Fig. 5 where the absorption is measured as the laser frequency is tuned across a single resonance. The Rabi excitation spectrum is shown at right, with a resulting linewidth of 2.1(2) Hz ($Q \sim 2\times10^{14}$) [21], near the ~1.8 Hz Fourier limit

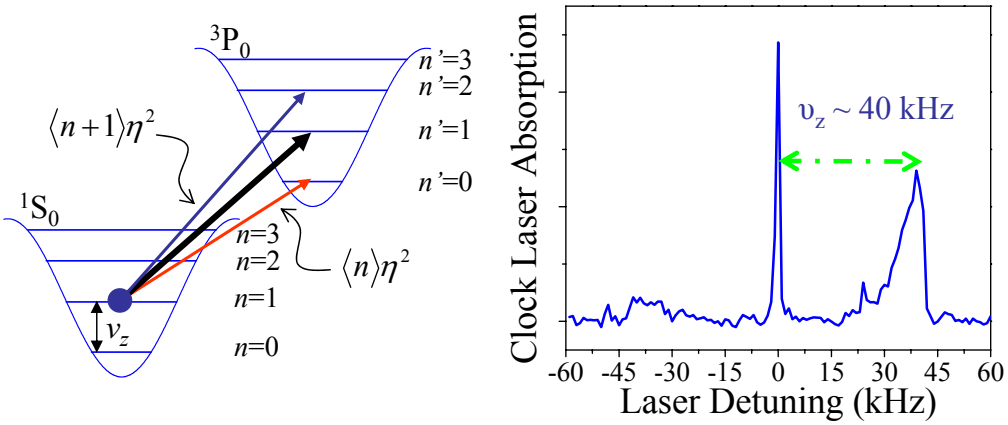

Fig. 4. – Spectroscopy of Sr atoms in a one dimensional lattice. (Left) Cartoon of spectroscopy in an optical lattice. Changes in motional state n during spectroscopic excitation results in modulation sidebands detuned from the natural resonance by the trap oscillation frequency. In the Lamb-Dicke regime, the amplitudes of the red- and blue-detuned sidebands are suppressed relative to the carrier by a factors of $\sim < n > \eta^2$ and $< n+1 > \eta^2$ respectively, where η is the Lamb-Dicke parameter. (Right) Absorption spectrum of lattice confined Sr atoms when the clock transition is strongly saturated. The sideband spectrum can be used to measure the trap parameters and atomic temperature as discussed in the text. Here the trap frequency is observed to be near 40 kHz, corresponding to $\eta \sim 0.3$.

set by the 500-ms interrogation time. This coherent atom-optical field interaction over a time period of nearly 1 s suggest that the optical trap does not decohere the atomic sample significantly over that time. Laser frequency noise prevents us from going to longer probe times as the beat between the two 698 nm lasers broadens to nearly 2 Hz when integrated over the relevant timescale for the line scan (∼30 s). Although the line Q presented here is limited by the laser linewidth, to our knowledge it is the highest Q ever observed in coherent spectroscopy. Ramsey spectroscopy has also been performed, as shown on the left side of Fig. 5. The Doppler-free absorption and long interaction time provided by the lattice confinement allows use of long, low-intensity pulses for the Ramsey sequence, resulting in simple spectra with a small number of fringes. This simplifies the identification of the central fringe compared to that of free falling clouds of cold atoms.

6. – Nuclear Structure Effects

The hertz-linewidth spectroscopy gives us the capability to investigate the nuclear spin-related effects for the clock transition. The presence of a nuclear spin ($I = 9/2$) in the ^{87}Sr isotope plays an important role in the development of an optical lattice clock [15, 29]. The nuclear spin provides a weak state mixing channel between the $^3P_0$ state and the $^1P_1$ and $^3P_1$ states. This mixing mechanism is responsible for the weakly allowed clock transition (∼1 mHz), but the hyperfine structure also leads to a few systematic effects that need to be understood and controlled. The mixing slightly modifies the magnetic moment of the $^3P_0$, resulting in a differential Landé g-factor, δg, for the clock transition, and therefore a first order Zeeman shift sensitivity [48, 49]. The nuclear spin also results in a small sensitivity of atomic level shifts to light polarization [50]. The origin

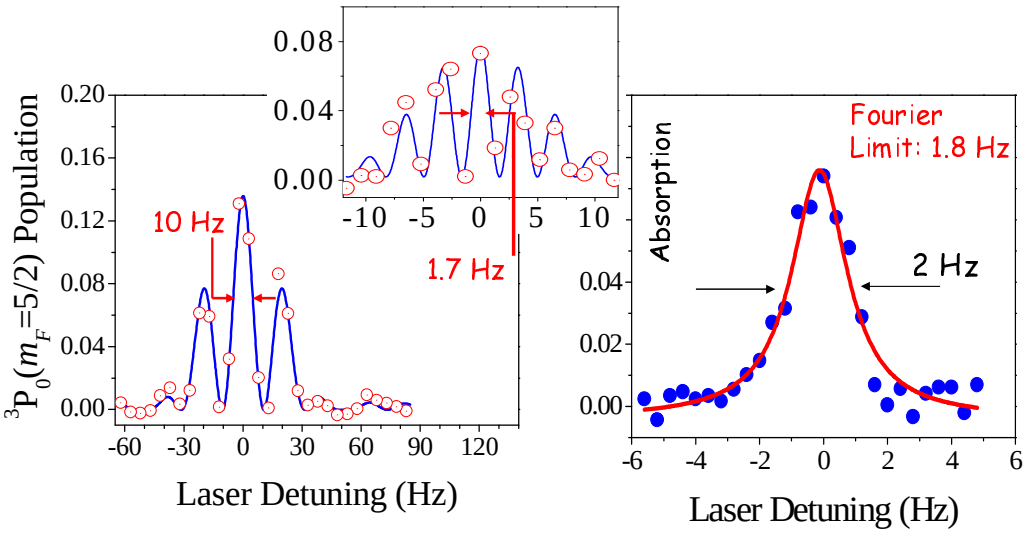

Fig. 5. – Ultra high resolution spectroscopy inside the magic wavelength optical lattice. Spectra of the clock transition ($m_F = 5/2$) are obtained under weak excitation and with the Zeeman degeneracy removed. The Ramsey spectrum on the left has a 10 Hz wide central feature, and the Rabi spectrum on the right is 2 Hz wide, in agreement with what is expected for the given probing and free evolution times. The inset shows a Ramsey spectrum collected with a longer free evolution time, and the central feature is 1.7 Hz wide.

and magnitude of these spin-related field sensitivities are discussed in detail elsewhere [29, 39].

For π transitions ($\Delta m_F = 0$), the frequency shift in an optical lattice with trap depth U_T, linearly polarized along the quantization axis defined by a bias magnetic field B, is given by,

$$\Delta\nu = -\left(\Delta\kappa^S - \Delta\kappa^T \frac{99}{4}\right)\frac{U_T}{E_R} - \left(\Delta\kappa^V m_F \xi\delta\varphi + \Delta\kappa^T 3m_F^2\right)\frac{U_T}{E_R} - \delta g m_F \mu_0 B. \quad (2)$$

Here κ represents the polarizability (and $\Delta\kappa$ the difference between $\alpha_{^1S_0}$ and $\alpha_{^3P_0}$) when the laser intensity is characterized by the ratio of U_T/E_R, where E_R is the energy associated with a lattice photon recoil. This is a natural way to describe the light shift as U_T can be directly measured using sideband spectroscopy. Then, $\Delta\kappa^S$, $\Delta\kappa^V$, and $\Delta\kappa^T$ represent respectively frequency shift coefficients proportional to the differential scalar, vector, and tensor polarizabilities of $^1S_0$ and $^3P_0$, given in units of Hz/(U_T/E_R). ξ is the degree of circular polarization of the trapping beams and $\delta\varphi$ is the misalignment between the quantization axis and light polarization. In the experimental setup used in this work $\xi \approx \delta\varphi \approx 0$. The basic principle of the lattice clock technique is to tune the lattice wavelength (and hence the polarizabilities) such that the intensity-dependent frequency shift terms are reduced to zero. Due to the m_F-dependence of the shift described in the second term of Eq. 2, the Stark shifts cannot be completely compensated for all of the sublevels simultaneously. The significance of this effect depends on the magnitude of the tensor and vector terms relative to the scalar term, which is small for the nuclear spin. With a spin-polarized atomic sample, the vector dependence can be eliminated by

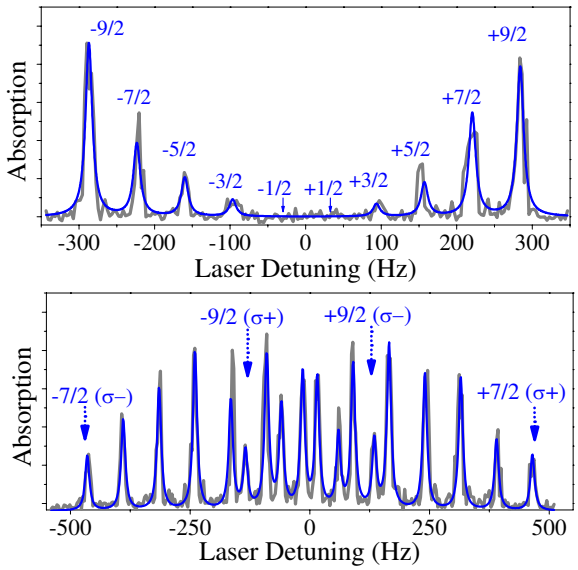

Fig. 6. – Spectroscopy of the clock transition in the presence of a bias magnetic field. (top) Absorption spectrum when the linear polarized probe light is polarized along the quantization axis defined by $B = 0.58$ G . The large nuclear spin ($I = 9/2$) results in ten possible π transitions with amplitudes consistent with Clebsch-Gordan coefficients. (bottom) Absorption spectrum with the probe polarized orthogonally to the bias field of $B = 0.69$ G. In this case, nine σ^+ and σ^- transitions are observed. Transition labels represent the ground state m_F value. From the spectral pattern it can be determined unambiguously that the nuclear spin state mixing increases the size of the $^3P_0$ g-factor.

taking the average of measurements based on two opposite-signed $|m_F|$ sublevels. The tensor dependence can be absorbed into the definition of the magic wavelength since only a single $|m_F|^2$ term is involved. The third term in Eq. 2 gives the linear Zeeman sensitivity due to the modified magnetic moment of $^3P_0$. The hyperpolarizability [38] and the second order Zeeman shifts [29] are not included here since they are of negligible magnitudes.

When operating near the magic wavelength, the most significant clock shift is that of the differential g-factor. To explore the magnitude of δg we have performed NMR-like measurements on various m_F sublevels of the clock transition in the presence of a bias magnetic field [21, 29]. The upper panel of Fig. 6 shows an absorption spectrum in the presence of a bias field using linearly polarized light to drive ten possible π-transitions. While the π transitions allow a simple determination of δg, the measurement requires a careful calibration of the magnetic field and a precise control of the probe laser frequency over $\sim$500 s that is required to produce the scan shown in the figure. Furthermore, the measurement can not be used to determine the sign of δg, leaving it ambiguous as to whether the magnetic moment of $^3\mathrm{P}_0$ is larger or smaller than that of $^1\mathrm{S}_0$. To make a more definitive measurement, the probe laser can instead be polarized perpendicular to the lattice polarization axis. This configuration results in excitations of nine σ^+ and nine σ^- transitions ($\Delta m_F = \pm 1$). Hence, 18 spectral features are observed as shown in the lower panel of Fig. 6. The additional information provided by the two sets of spectra

TABLE I. – *Measured nuclear spin related field sensitivities for the ^{87}Sr clock transition. For details on the determination of the coefficients, see Ref. [29, 39].*

Sensitivity	Value	Units
$\Delta_B^{(1)}/m_F B$	-108.4(4)	Hz/G
$\Delta\kappa^T$	$6(20)\times10^{-4}$	$\mathrm{Hz}/(U_T/E_R)$
κ_{3P0}^T	$5(10)\times10^{-4}$	$\mathrm{Hz}/(U_T/E_R)$
$\Delta\kappa^V\xi\delta\varphi$	$0(6)\times10^{-4}$	$\mathrm{Hz}/(U_T/E_R)$

allow measurement of δg without extra calibration of the magnetic field and without any sign ambiguity, provided that the ground state g-factor is known. Using data such as that shown here, δg ($\times\mu_0$, where μ_0 is the Bohr magneton over Planck's constant h) has been determined experimentally to be -108.4(4) Hz/G [29]. By examining the δg spectrum for the m_F^2 and U_T dependance on the line splitting, upper limits for the tensor and vector light shifts can be extracted.

Table I summarizes the measured sensitivities to magnetic fields and the lattice potential that relate to the presence of nuclear spin. The small upper limit for the tensor shift suggests that the m_F dependence of the magic wavelength should be nearly negligible in current experiments. The vector shift limit is specific to our apparatus since the alignment angle and polarization purity are near zero but the exact values unknown. The limits to the Stark shift coefficients for linear polarization at 813.4280(5) nm are given in units of $\mathrm{Hz}/(U_T/E_R)$. With the evaluation performed here, the differential g-factor is by far the most significant nuclear spin effect for the one-dimensional lattice clock, and must be addressed in any accuracy evaluations.

7. – Clock Accuracy Evaluation

Central to the development of any frequency standard is the characterization of possible systematic frequency shifts. In the case of the lattice clock, the primary systematic concerns include the a.c. Stark shifts from the trapping lattice, optical probe, and black body radiation, linear and quadratic Zeeman shifts, and possible collision shifts. Recently, two modes of operation for the ^{87}Sr lattice clock have been evaluated for accuracy, both of which allowed characterization of the frequency uncertainty to below 10^{-15}.

In the first method, spectroscopy of the clock transition is performed in the absence of a magnetic bias field. Under this condition the linear and quadratic Zeeman shift could be minimized provided that the residual magnetic field is sufficiently nulled. Operating at a lattice wavelength of 813.4280(5) nm, we determine that the a.c. Stark shift for the typical trap depth is $-2.5(6.0)\times10^{-16}$. The atomic collision shift is constrained to be below 3.3×10^{-16}. Each of these effects is consistent with zero and limited by the statistical uncertainty associated with hundreds of measurements. The Zeeman sensitivity is determined to be non-zero but less than 5.3×10^{-16} when the residual magnetic field is controlled to <5 mG. The total uncertainty for degenerate level spectroscopy, summarized in Table II, under our operating conditions is 9×10^{-16} [28].

The systematic uncertainties associated with lattice spectroscopy discussed above are for the most part limited by the statistical uncertainty of the measurement. The magnetic field sensitivity on the other hand is limited by the field calibration and needs to be addressed. To avoid the shift due to the linear Zeeman effect, the second mode of

TABLE II. – *Systematic frequency shift evaluations using degenerate and spin-polarized measurement schemes discussed in the text. Note that the typical operating parameters for the two cases differ and are described elsewhere [28, 17].*

	Degenerate (2006)		Spin-Polarized (2007)	
Systematic Effect	Corr. (10^{-16})	Unc. (10^{-16})	Corr. (10^{-16})	Unc. (10^{-16})
Lattice ac Stark	2.5	6.0	-2.3	0.5
Hyperpolarizability	-0.13	0.13	-0.2	0.2
698 Probe ac Stark	-0.2	1.2	0.2	0.1
BBR Stark	54.4	1.6	52.1	1.0
1st order Zeeman	0	5.3	0.2	0.2
2nd order Zeeman	0	.002	0.2	0.02
Density	-0.1	3.3	8.9	0.8
Line pulling	–	–	0	0.2
Servo error	–	–	0	0.5
Total	56.5	8.8	59.1	1.5

operation employs spin-polarized samples where atoms are optically pumped to the $m_F = \pm 9/2$ sublevels before spectroscopy. In this configuration, spectroscopy is performed in the presence of a small bias field. The average value of the two π-transitions ($m_F = \pm 9/2$) is used to determine the mean clock frequency that is independent of the magnetic bias field. This averaging technique also eliminates any residual vector light shifts as they are proportional to m_F as well. The tensor light shift becomes unimportant since a single $|m_F|$ value is used and the shift is automatically absorbed into the determination of the magic wavelength. Thus, the spin-polarized method should allow greater accuracy than the degenerate case.

With the main concern in the uncertainty budget eliminated, the evaluation of accuracy can be further improved by decreasing the statistical uncertainty in the measurement of various frequency shifts. To improve the precision of the evaluation, systematic shifts are measured against a high-precision Ca optical clock at NIST [51] using a stabilized fiber link that connects the JILA and NIST laboratories [6]. Figure 7 shows the results of a direct optical comparison between the spin-polarized ^{87}Sr lattice clock and the Ca clock. The stability at 1 s is 3×10^{-15} and a precision of 3×10^{-16} is achieved in only 200 seconds of averaging. With the combination of increased precision and the spin-polarized method, the Sr systematics have now been evaluated at the level of 1.5×10^{-16} (see Table II) [17, 52].

8. – Absolute Frequency Measurements

With the systematic frequency shifts well characterized, the remaining issue is measurement of the absolute frequency of the Sr lattice clock relative to a Cs primary standard. At JILA, absolute frequency measurements are performed using a NIST H-maser that is calibrated by the Cs fountain [44]. The microwave reference is transferred from NIST to JILA using a stabilized optical fiber link [46], allowing direct clock comparison using a fs-comb. The uncertainty in the Sr-maser comparison averages down as $3\times10^{-13}\tau^{-1/2}$, requiring long averaging times to reach the Sr uncertainty limit.

Using the degenerate sublevel system, a 24-hour run of measurements made on the

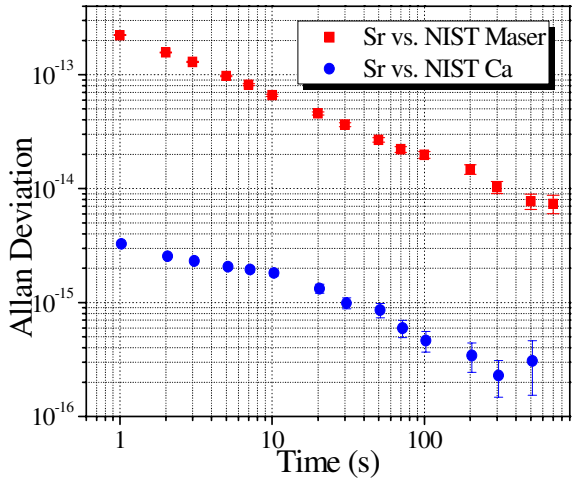

Fig. 7. – Allan deviation of two clock comparisons. Remote comparison of the Sr lattice clock and the NIST H-maser (squares) via an stabilized optical fiber link provides a stability of $3\times10^{-13}\tau^{-1/2}$, allowing highly accurate absolute optical frequency measurements. An all optical comparison between the JILA Sr clock and the NIST Ca clock (circles) reveals an improved stability below $4\times10^{-15}\tau^{-1/2}$, allowing rapid measurements of systematic effects for improved accuracy evaluations.

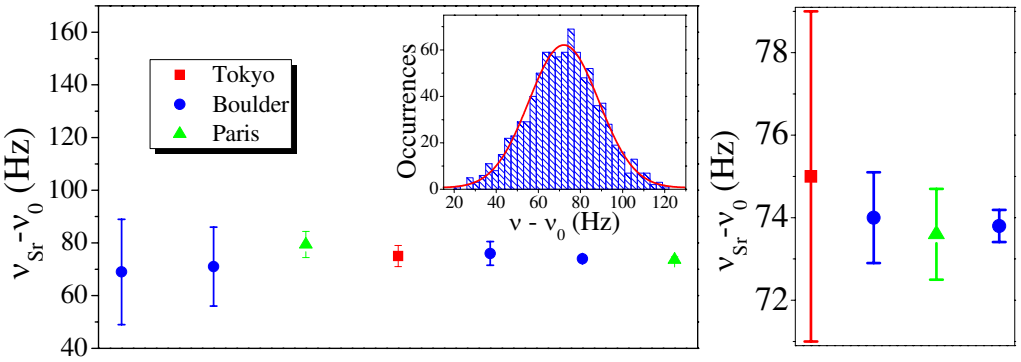

Fig. 8. – Absolute frequency measurements of the $^1S_0-^3P_0$ transition in ^{87}Sr in an optical lattice. (left) Published measurements from the groups of Boulder (circles) [24, 53, 54, 28], Paris (triangles) [25, 30], and Tokyo (squares)[27] relative to an offset of $\nu_0 = 429\ 228\ 004\ 229\ 800$ Hz. Inset shows a histogram of the frequency measurements and a Gaussian fit of the data that corresponds to the last Boulder point shown in the main view graph. This measurement has a total uncertainty of 2.5×10^{-15}. (right) A closer view of the most recent measurements of the three groups shows the excellent agreement between the different lattice clocks. The final Boulder data point on the plot (not shown in the left panel) has an uncertainty of only 9×10^{-16} and is in excellent agreement with the previous values [55].

^{87}Sr clock transition determines its frequency to be 429,228,004,229,874.0 ± 1.1 Hz [28]. The total uncertainty of 2.5×10^{-15} is dominated by the statistical uncertainty in the comparison (1.4×10^{-15}) and the maser calibration (1.7×10^{-15}). The data for this clock comparison is summarized as a histogram of frequency measurements in the inset of Fig. 8. The main plot on the left of Fig. 8 summarizes the recent absolute frequency measurements made by the groups at JILA (circles) [24, 53, 54, 28], in Paris (triangles) [25, 30], and in Tokyo (squares) [27]. The excellent agreement over the past two years between three independent groups speaks strongly for the ^{87}Sr lattice clock as a frequency standard.

The right panel in Fig. 8 shows a closer view of the most recent measurements from each group. The agreement between these measurements is at an unprecedented level for optical frequency standards, with the Boulder and Paris group agreeing below 1×10^{-15}. The last data point included in this panel represents a more recent measurement made at JILA using the spin-polarized operation of the clock over a 48-hour time window when the Cs fountain is operated simultaneously. In this improved measurement, the total frequency measurement uncertainty reaches below 9×10^{-16} and the frequency value agrees with our previous measurement made one year earlier to better than 5×10^{-16} [55]. Agreement at this level over long spans of time and between multiple labs is an essential step in the development of a frequency standard. The rapid progress and excellent agreement in just a few years of progress should make the Sr lattice clock an exciting candidate for future redefinition of the SI second.

9. – Fundamental Physics

The unprecedented level of agreement on an optical clock frequency can be used to test fundamental physics questions. Among these, possible time-dependent variations of fundamental constants have received particular attention. One example review is provided in Ref. [56]. By combining Sr clock data from the Boulder, Paris, and Tokyo groups we obtain a global record of Sr $^1S_0-{}^3P_0$ frequency measurements spanning the last three years with a good coverage of the entire time window. This record can be analyzed for variations to constrain temporal changes of fundamental constants such as the fine-structure constant $\alpha = e^2/(4\pi\epsilon_0\hbar c)$ or the electron-proton mass ratio $\mu = m_e/m_p$.

The absolute frequency measurement against the Cs standard makes any optical clock frequency depend on α and μ in a species-specific way. These dependencies are determined by relativistic correction factors that depend on the atomic mass and the combination of atomic states used for the clock [57, 58]. Thus, data from one species such as Sr has to be combined with data from other species, such as Hg [59], Yb [60, 61], and Hydrogen [62], to find numerical constraints on the fractional variations $\delta\alpha/\alpha$ and $\delta\mu/\mu$. The yearly fractional drift x_j of each species j contributes a linear constraint of the form $x_j = -c^j_\alpha \frac{\delta\alpha}{\alpha} - \frac{\delta\mu}{\mu}$, with species sensitivity constant c^j_α. The constraints from each species are shown in Fig. 9. Using standard linear regression techniques detailed in Ref. [63], we find [64],

$$\delta\alpha/\alpha = (-3.1 \pm 3.0)\times10^{-16}/\text{yr},\ \delta\mu/\mu = (1.5 \pm 1.7)\times10^{-15}/\text{yr}. \tag{3}$$

In a similar manner, fundamental constants could also depend on the ambient gravitational field. Such a dependence would cause sidereal variation in the clock frequency as Earth revolves around the Sun on an elliptical orbit. To lowest order in the ellipticity, such a variation would be sinusoidal. The amplitude of a corresponding fit to the

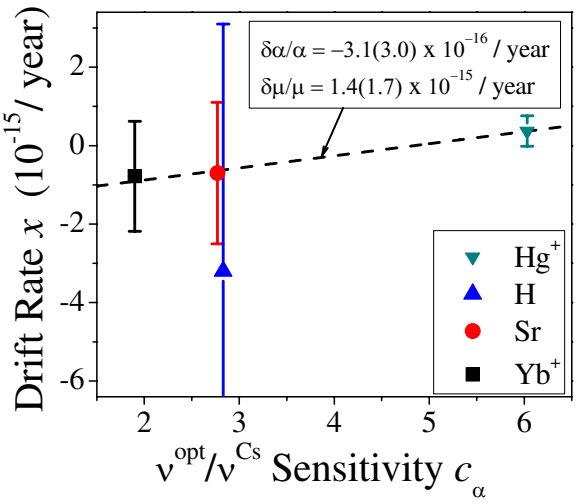

Fig. 9. – The Sr lattice clock data (circle) can be combined with the Hg^+ (inverted triangle) [59], Yb^+ (square) [61], and H (triangle) [62] data to constrain drifts of α and μ. Fractional frequency drift rates x of different optical clocks against Cs primary standards are plotted vs. species sensitivity constant c_α. A linear fit determines limits on yearly drift rates $\delta\alpha/\alpha$ and $\delta\mu/\mu$.

combined data record then limits the coupling of fundamental constants η to the gravitational potential, expressed by limits on dimensionless coupling constants k_η [65]. As discussed above, the comparison against the Cs standard makes an optical clock sensitive to variation in α and μ (expressed by k_α and k_μ here) and data from different species must be combined to extract constraints. Hydrogen masers measured against the Cs standard are also sensitive to variation in the light quark mass, adding another coupling constant k_q [58]. By combining the Sr results with data from Hg^+ and the H-maser, we find [64]

$$(4) \qquad k_\alpha = (-2.3 \pm 3.1) \times 10^{-6},\ k_\mu = (1.1 \pm 1.7) \times 10^{-5}\ k_q = (1.7 \pm 2.7) \times 10^{-5}.$$

These constraints are the most stringent to date and we conclude that there is no coupling of α, μ and light quark mass to gravity at the current level of accuracy.

10. – Precision measurement and control with ultracold molecules

The measurement precision made possible with state-insensitive optical traps extends beyond Sr and other alkaline earth atoms. For instance, these optical traps can be applied directly to cold molecule physics, which is foreseen to play increasingly important roles in novel quantum dynamics, precision measurement, and ultracold collisions and chemical reactions. Cold molecules can be created through photoassociation processes using a weak electronic transition. The narrow transition linewidth requires precise and long-duration atom-light interactions and this condition is fulfilled in a state-insensitive trap [66]. Second, ground-state molecules can be confined in a lattice field where two specific molecular vibrational levels have the same polarizability, thus enabling the operation of a high-accuracy optical molecular clock [67].

We have carried out narrow-line photoassociation studies with ^{88}Sr near the $^1S_0-^3P_1$ dissociation limit [66]. The lack of nuclear spins (and simple correspondence to theory) makes ^{88}Sr ideal for photoassociation via the narrow spin-forbidden transition. The wavelength of a state-insensitive lattice trap for the $^1S_0-^3P_1$ transition is ∼914 nm, permitting a recoil- and Doppler-free photoassociation process. The 15 kHz natural width of the molecular line can resolve every vibrational level near dissociation and has so far allowed observation of nine least-bound molecular states. The line shapes are sensitive to thermal effects even at 2 μK ultracold temperatures and to zero-point shifts by the optical lattice confinement. The combination of a narrow width of the least-bound state and its strong coupling to the scattering state should allow efficient tuning of the ground state scattering length with the optical Feshbach resonance technique. The other important feature of this narrow-line photoassociation is the large Franck-Condon overlap between the bound-state wave functions in the excited and ground electronic states. This good overlap leads to efficient productions of ultracold ground-state molecules.

Ultracold nonpolar Sr_2 molecules confined in a lattice can serve as a basic system for precision measurement of the drift of fundamental physical constants. The scalar nature of the molecular vibrational levels in the electronic ground state makes it ideal to find a magic lattice wavelength for matching polarizabilities of two vibrational levels. This strategy permits precise measurement of the vibrational energy interval in the electronic ground state of the dimer. This molecular clock system is particularly suitable for measurements of the possible variation of the proton-electron mass ratio. The expected constraint reaches 1×10^{-15}/year [67], similar to that provided by atomic frequency metrology. However, tests based on molecular vibration frequencies provide far more independence from theory models than atomic tests.

* * *

We gratefully acknowledge M. H. G. de Miranda and M. J. Martin for the frequency comb clockwork, T. Ido, T. Loftus, and J. Thomsen for contributions to the Sr lattice experiment, T. Zanon, E. Arimondo, and C. Greene for atomic theory, P. Julienne and S. Kotochigova for molecular theory, M. Notcutt and J. L. Hall for stable lasers, and J. Bergquist, S. Diddams, T. Fortier, S. Jefferts, C. Oates, T. Parker of the NIST Time and Frequency Division for collaborations and discussions. The work at JILA is supported by NIST, NSF, DARPA, and ONR.

REFERENCES

[1] B. C. Young *et al.*, Phys. Rev. Lett. **82**, 3799 (1999).
[2] A. D. Ludlow *et al.*, Opt. Lett. **32**, 641 (2007).
[3] T. W. Hänsch, Rev. Mod. Phys. **78**, 1297 (2006).
[4] J. L. Hall, Rev. Mod. Phys. **78**, 1279 (2006).
[5] S. T. Cundiff and J. Ye, Rev. Mod. Phys. **75**, 325 (2003).
[6] S. M. Foreman *et al.*, Phys. Rev. Lett. **99**, 153601 (2007).
[7] R. H. Dicke, Phys. Rev. **89**, 472 (1953).
[8] D. Leibfried, R. Blatt, C. Monroe, and D. Wineland, Rev. Mod. Phys. **75**, 281 (2003).
[9] A. Ashkin, J. M. Dziedzic, J. E. Bjorkholm, S. Chu, Opt. Lett. **11**, 288 (1986).
[10] S. Chu, J. E. Bjorkholm, A. Ashkin, A. Cable, Phys. Rev. Lett. **57**, 314 (1986).
[11] J. Ye, D. W. Vernooy, and H. J. Kimble, Phys. Rev. Lett. **83**, 4987 (1999).
[12] H. Katori, T. Ido, and M. Kuwata-Gonokami, Jour. Phys. Soc. Japan **68**, 2479 (1999).
[13] J. Ye, H. J. Kimble, and H. Katori, Science, to be published (2008).

[14] R. Miller *et al.*, J. Phys. B - At. Mol. Opt. Phys. **38**, S551 (2005).
[15] H. Katori *et al.*, Phys. Rev. Lett. **91**, 173005 (2003).
[16] W. H. Oskay *et al.*, Phys. Rev. Lett. **97**, 020801 (2006).
[17] A. D. Ludlow *et al.*, submitted for publication (2008).
[18] D. J. Wineland and Wayne M. Itano, Phys. Rev. A **20**, 1521 (1979).
[19] D. J. Wineland, W. M. Itano, J.C. Bergquist, and R. G. Hulet, Phys. Rev. A **36**, 2220 (1987).
[20] L. Hollberg *et al.*, IEEE J. Quant. Electron. **37**, 1502 (2001).
[21] M. M. Boyd *et al.*, Science **314**, 1430 (2006).
[22] R. J. Rafac *et al.*, Phys. Rev. Lett. **85**, 2462 (2000).
[23] M. Takamoto *et al.*, Nature **435**, 321 (2005).
[24] A. D. Ludlow *et al.*, Phys. Rev. Lett. **96**, 033003 (2006).
[25] R. Le Targat *et al.*, Phys. Rev. Lett. **97**, 130801 (2006).
[26] Z. W. Barber *et al.*, Phys. Rev. Lett. **96**, 083002 (2006).
[27] M. Takamoto *et al.*, J. Phys. Soc. Japan **75**, 10 (2006).
[28] M. M. Boyd *et al.*, Phys. Rev. Lett. **98**, 083002 (2007).
[29] M. M. Boyd *et al.*, Phys. Rev. A **76**, 022510 (2007).
[30] X. Baillard *et al.*, arXiv:0710.0086v1 (2007).
[31] J. L. Hall, M. Zhu, and P. Buch, J. Opt. Soc. Am B **6**, 2194 (1989).
[32] H. Katori, in *Proceedings of the 6th Symposium on Frequency Standards and Metrology*, P. Gill, Ed. (World Scientific, St. Andrews) pp. 323-330 (2002).
[33] R. Santra, K. V. Christ, and C. H. Greene, Phys. Rev. A **69**, 042510 (2004).
[34] S. G. Porsev and A. Derevianko, Phys. Rev. A **69**, 042506 (2004).
[35] H. Katori, T. Ido, Y. Isoya, and M. Kuwata-Gonokami, Phys. Rev. Lett. **82**, 1116 (1999).
[36] T. H. Loftus *et al.*, Phys. Rev. Lett. **93**, 073003 (2004).
[37] T. H. Loftus *et al.*, Phys. Rev. A **70**, 063413 (2004).
[38] A. Brusch *et al.*, Phys. Rev. Lett. **96**, 103003 (2006).
[39] M. M. Boyd, Ph.D. Thesis, University of Colorado (2007). Available online at http://jilawww.colorado.edu/YeLabs/pubs/theses.html.
[40] P. Lemonde and P. Wolf, Phys. Rev. A **72**, 033409 (2005).
[41] M. Notcutt *et al.*, Opt. Lett. **30**, 1815 (2005).
[42] K. Numata, A. Kemery, and J. Camp, Phys. Rev. Lett. **93**, 250602 (2004).
[43] M. Notcutt *et al.*, Phys. Rev. A **73**, 031804 (2006).
[44] T. P. Heavner *et al.*, Metrologia **42**, 411 (2005).
[45] J. Ye *et al.*, J. Opt. Soc. Am B **20**, 1459 (2003).
[46] S. M. Foreman *et al.*, Rev. Sci. Inst. **78**, 021101 (2007).
[47] T. M. Fortier, A. Bartels, and S. A. Diddams, Opt. Lett. **31**, 1011 (2006).
[48] B. Lahaye and J. Margerie, J. Physique **36**, 943 (1975).
[49] T. Becker *et al.*, Phys. Rev. A **63**, 051802 (2001).
[50] M. V. Romalis and E. N. Fortson, Phys. Rev. A **59**, 4547 (1999).
[51] G. Wilpers *et al.*, Appl. Phys. B **85**, 31 (2006).
[52] A. D. Ludlow, Ph.D. Thesis, University of Colorado (2008). Available online at http://jilawww.colorado.edu/YeLabs/pubs/theses.html.
[53] M. M. Boyd *et al.*, in *Proceedings of the 20th European Frequency and Time Forum*, Braunschweig, Germany, March 27-30, pp. 314-318 (2006).
[54] J. Ye *et. al.*,*Atomic Physics 20, Proceedings of the XX International Conference on Atomic Physics; ICAP 2006*. C. Roos, H. Häfner, and R. Blatt editors. AIP, pp 80-91 (2006).
[55] G. K. Campbell *et al.*, in preparation (2008).
[56] S. Lea, Rep. Prog. Phys. **70**, 1473 (2007).
[57] E. J. Angstmann, V. A. Dzuba, and V. V. Flambaum, arXiv:0407141v1 (2004).
[58] V. V. Flambaum and A. F. Tedesco, Phys. Rev. C **73**, 055501 (2006).
[59] T. M. Fortier *et al.*, Phys. Rev. Lett. **98**, 070801 (2007).
[60] E. Peik *et al.*, Phys. Rev. Lett. **93**, 170801 (2004).
[61] E. Peik *et al.*, arXiv:0611088 (2006).
[62] M. Fischer *et al.*, Phys. Rev. Lett. **92**, 230802 (2004).

[63] N. Kolachevsky *et al.*, to be published (2008).
[64] S. Blatt *et al.*, submitted for publication (2008).
[65] V. V. Flambaum, Int. J. Mod. Phys. A **22**, 4937 (2007).
[66] T. Zelevinsky *et al.*, Phys. Rev. Lett. **96**, 203201 (2006).
[67] T. Zelevinsky, S. Kotochigova, and J. Ye Phys. Rev. Lett., in press (2008).